

"Fat" Rays in Three Dimensional Media to Approximate a Broadband Signal Propagation

Dmitry Neklyudov(✉) and Maxim Protasov

Institute of Petroleum Geology and Geophysics SB RAS, prosp. acad. Koptuga 3, Novosibirsk 630090, Russia
neklyudovda@ipgg.sbras.ru

Abstract. The paper presents a simple and robust approach for calculating frequency-dependent rays in three-dimensional media. The proposed ray tracing procedure simulates propagation of locally plane fragment of a wave front. Ray properties depend on velocity distribution in some sub-volume around the ray and on wavelength at each point. We provide a numerical comparison of "fat" rays approach with the "exact" Helmholtz solver using complex 3D SEG salt model. This comparison show promise of using the concept of "fat" rays in 3D seismic data processing, i.e. comparison show that "fat" rays approach needs up to several orders less resources than Helmholtz solver, while the error between "fat" rays wave filed and "exact" solution does not exceed several percent.

Keywords: Fat rays · Ray method · Broadband signal · Green function

1 Introduction

The ray method [1, 2] play an important role in seismic data processing. Its main application is to calculate the ray paths and corresponding travel times of seismic waves. It is also used for the computation of wave fields in models of moderate complexity. The classical ray theory is formulated using a high-frequency approximation of signal propagation processes. This fact produces the main limitation of all ray-based methods. Classical ray method does not take into account the fact that actual seismic signals are broadband and their spectrum are limited. A high-frequency approximation often leads to a non-physical behavior of the rays if there are significant velocity variations in a model [3, 4]. On nonplanar surfaces, the standard rays disperse abruptly and as a result, shadow zones appear in the model (i.e. the regions where the rays do not pass at all). Propagation of the signals with limited spectrum depends on velocity distribution within certain volume around the ray. These volumes are called as "Fresnel volumes". Dominant frequency of the signal determines the width of the Fresnel volume. The real signals are affected by velocity variations within the Fresnel volume [5, 6]. A number of methods are developed to go beyond the standard ray method based on high frequency approximation. The main idea behind these approaches is to consider the impact of the

© The Author(s), under exclusive license to Springer Nature Switzerland AG 2023
O. Gervasi et al. (Eds.): ICCSA 2023, LNCS 13957, pp. 110–124, 2023.
https://doi.org/10.1007/978-3-031-36808-0_8

Fresnel zone on travel times and ray paths [7–14]. It allows to weaken the impact of the high-frequency approximation. As a result, it is possible to calculate the reliable rays in fairly complex velocity models. The principal disadvantage of the proposed approaches is the complexity of the calculations, especially in the three-dimensional case. Original approach for approximating the propagation of broadband seismic signals in complex environments was proposed in [8] where it was called "the wavelength-smoothing technique". The key point there is the fact that velocity used for ray tracing is determined by smoothing actual velocity along the normal to the ray at the current point over an aperture proportional to the wavelength. In the limiting case when the wavelength becomes infinite small, the method reduces to the standard rays described by classical ray theory. In [15], we considered this method in 2D case and proved that it might be quite promising in some seismic exploration applications. Specifically, we found that these rays can be very effective in calculating travel times in the presence of salt intrusion in a model. This work is an extension of [15] to three dimensions. We propose quite simple and robust algorithm to construct frequency dependent rays in complex 3D media. It consists of two main ingredients: 1) the velocity wavelength-smoothing technique along a 2D wave front; 2) movement of a number of points located on a plane wave front' fragment in some vicinity of a ray to determine the wave front orientation at a next point on the ray. During ray tracing process a local plane fragment of the wave front moves. Thus, ray's orientation depends on velocity distribution in some sub-volume around the ray. This is why we called such rays as "fat" rays. The term "fat" rays is already widely used in seismic [16]. Usually it means a standard ray attributed with corresponding first Fresnel zone. In our case the sense of the term is a little bit different.

The paper is organized in the following way. First, we describe simple algorithm how to construct a frequency-dependent ray in three dimensions. We then describe an approach for interpolating travel times from the irregular points on the rays to the regular 3D grid. Next, we briefly describe an approach we use to calculate ray based amplitudes. Finally, we give two numerical examples and demonstrate that "fat" rays are more stable than standard rays in complex 3D models. We conclude that the "fat" rays can provide reliable travel times and amplitudes when the standard ray method fails.

2 Method

2.1 "Fat" Ray Construction

"Fat" ray tracing is based on two main concepts. First is the wavelength-smoothing technique proposed in [8]. This technique allows to calculate locally smoothed velocity in vicinity of a ray. Smoothing is performed in particular direction, namely along a wave front, i.e. in a plane which is orthogonal to the current ray's propagation direction. The second concept is the local control points movement which is used to determine a ray propagation vector at a next point on the ray. As an input of the procedure, we define auxiliary parameter υ (measured in Hz), which is called "frequency" of the ray. This parameter defines the sensitivity of the ray to velocity variations. Two take-off angles φ_{AZ}, φ_{Dip} are also given. φ_{AZ} is the azimuthal angle (i.e. an angle between initial ray direction and X-axis in XY plane), φ_{Dip} is dip angle (i.e. an angle between initial ray direction and Z-coordinate axis). Let $\vec{x}_p = (x_p, y_p, z_p)$ is a current point on the ray

(central point). At this point, a unit tangent vector $\vec{s} = (s_X, s_Y, s_Z)$ is given which define a ray propagation direction at the current point. We construct a plane passes through the point $\vec{x}_p$ and orthogonal to the vector $\vec{s}$. In this plane, we cut a rectangular area ("patch"). The size of the rectangular is a function of local wavelength in the central point, $\lambda = \frac{v(\vec{x}_p)}{\upsilon}$ (see Fig. 1a). Local velocity value $v(\vec{x}_j)$ is defined in the regular grid of points in the patch (these points are shown as the blue stars in Fig. 1a). Smoothed velocity in the central point is calculated as

$$v_{sm}(\vec{x}_p, v) = \frac{\sum_{j=-N}^{N} w_j \cdot v(\vec{x}_j)}{\sum_{j=-N}^{N} w_j} \tag{1}$$

where w_j are the smoothing weights. As a smoother we choose 2D Gaussian function. The weights are given as:

$$w_j = \exp\left\{-\left(\frac{r_j}{\lambda \cdot \theta_{max} \cdot \alpha}\right)^2\right\}, \tag{2}$$

where r_j is a distance between the central point and the point $\vec{x}_j$ in the wavefront patch, predefined parameter θ_{max} (local wavelength percentage) determines the spatial size of the rectangular, parameter α is responsible for the shape of the Gaussian smoother. In the Fig. 2, we show how the Gaussian smoothing function (2) behaves in relation to the parameter α. When the parameter α is reduced, the smoothing function becomes narrower, concentrating near the center point. When increasing the parameter α, the Gaussian smoothing is reduced to simple averaging in the rectangular area.

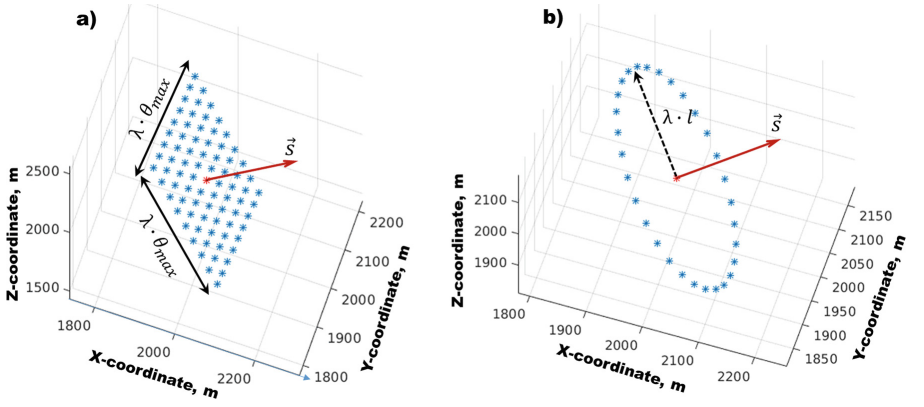

Fig. 1. a) Rectangular area ("patch") cut along a local wave front. Blue stars mark the points where velocity values are taken to calculate smoothed velocity at the central point (shown as a red star). Vector $\vec{s}$ denote current normal to the front (ray propagation direction). b) Control points taken around the central point. They are used calculating new normal to the front $\vec{s} + d\vec{s}$. (Color figure online)

To explain a meaning of the control points, we consider a circle lying in the same plane orthogonal to the current ray propagation direction vector $\vec{s}$. Radius of the circle

is also function of the local wavelength, $R = \lambda \cdot l$ (predefined parameter l controls the percentage of the local wavelength which one want to use). We choose a number of points lying on the circle with constant angular increments (see Fig. 1b). We shall refer to these points as "control" points. They are used for calculating vector $\vec{s} + d\vec{s}$ in the next point on the ray.

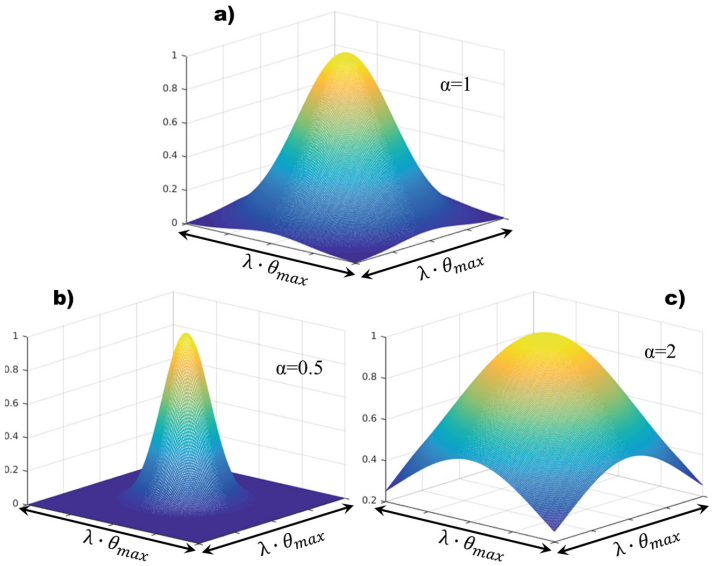

Fig. 2. 2D Gaussian functions used for velocity wavelength-smoothing along the front for different value of parameter α.

Let us define the time step along the ray as dt. To move along the "fat" ray we apply the following scheme (see Fig. 3).

1) We calculate the wavelength-smoothed velocity at the central point, $\overline{v}_p = v_{sm}(\vec{x}_p, v)$ using the formulas (1), (2). During the time interval dt, the central point $\vec{x}_p$ moves to the point $\vec{x}_p + d\vec{x}_p$, $d\vec{x}_p = (dx_p, dy_p, dz_p)$ along the vector $\vec{s}$:

$$dx_p = \overline{v}_p dt \cdot s_x, \quad dy_p = \overline{v}_p dt \cdot s_y, \quad dz_p = \overline{v}_p dt \cdot s_z, \tag{3}$$

It gives us a position of a next point on the ray. Now we need to determine new ray propagation direction vector $\vec{s}_{new}$ (or in other words, new local wavefront orientation).

2) For each control point, we calculate corresponding smoothed velocities using the same orthogonal plane as for the central point: $\overline{v}_j = v_{sm}(\vec{x}_j, v)$. For the same time interval dt each control point will travel different distances, $dx_j = \overline{v}_j dt \cdot s_x$, $dy_j = \overline{v}_j dt \cdot s_y$, $dz_j = \overline{v}_j dt \cdot s_z$. Control points in updated positions, $\vec{x}_j + d\vec{x}_j$ might not lie in the same plane. We define numerically a plane which is closest to all points $\vec{x}_j + d\vec{x}_j$ in the least-squares sense. Thus, we solve the classical three-dimensional linear regression problem. As a result, new ray direction vector $\vec{s}_{new}$ is defined. We attach $\vec{s}_{new}$ to the new central point position $\vec{x}_p + d\vec{x}_p$ and repeat the process. There is

a step-by-step movement along the ray. Note that the "fat" ray tracing is performed in a certain volume of the medium. Simultaneous movement of all control points determines the next orientation of the front.

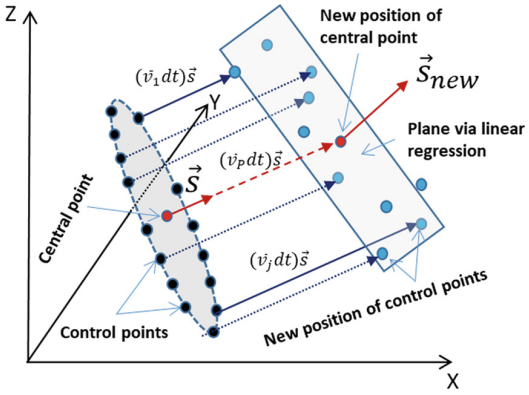

Fig. 3. Scheme of "fat" ray tracing.

2.2 Ray Travel Time Interpolation in 3D Regular Grid

When constructing rays, we determine the travel times at the points of the medium through which each ray passes. These points are quite irregular. For seismic applications, ray-based travel times must often be evaluated within a standard 3D grid. Such an array, consisting of the first arrival travel times given in the regular grid points, is called a travel time table.

Let we have constructed the number of rays for a large set of take-off angles. We presume that the rays cover the whole model. For each ray, we have a set of travel times at each point of the ray: $T_i^j(x_i^j, y_i^j, z_i^j)$, where $j = 1, \ldots, N_{rays}$ is an index of the ray, i is an index of a point on the ray, $i = 1, \ldots, N_{segm}^j$, N_{segm}^j is a total number of ray segment for jth ray. We need to make a map $T_i^j\left(x_i^j, y_i^j, z_i^j\right) \rightarrow T_{table}(x_k, y_l, z_m)$ for all j, where T_{table} are traveltimes given in the regular grid points x_k, y_l, z_m ($k = 1, \ldots, N_X$; $l = 1, \ldots, N_Y$;$m = 1, \ldots, N_Z$).

Consider successively the ray tubes, which are formed by three adjacent rays, first with the take-off angles $(\varphi_{AZ}, \varphi_{Dip})$, second $(\varphi_{AZ}, \varphi_{Dip} + d\varphi_{Dip})$, third $(\varphi_{AZ} + +d\varphi_{AZ}, \varphi_{Dip})$, where φ_{AZ} is azimuthal take-off angle, φ_{Dip} is dip take off angle, $d\varphi_{AZ}$, $d\varphi_{Dip}$ are corresponding angles increments. A ray tube may be decomposed into elementary prismatic cells which bottom corresponds to travel time T_j and top corresponds to $T_{j+1} = T_j + dt$ (see Fig. 4). Next, a parallelepiped which cover the prismatic cell with the regular grid points is determined. Every regular grid point of the parallelepiped domain is verified to be inside the prism cell. If so, the travel times at the prism cell vertices (marked as 11, 21, 31, 12, 22, 32 in the Fig. 4) are interpolated at the grid point using the method proposed in [17]. Overwise, the grid point gets ignored from consideration at the current stage. It is repeated for each ray cell and each ray tube. As a result,

a regular travel time table is constructed if the model has been illuminated by the rays adequately.

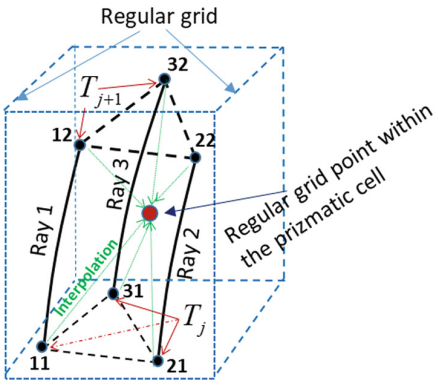

Fig. 4. Scheme of ray travel times interpolation to a regular grid.

2.3 Green's Function Calculation

In seismic imaging, it is often necessary to calculate Green's functions for scalar wave equation or its frequency domain counterpart, Helmholtz equation:

$$\Delta G(\vec{x}, \vec{x}_S; \omega) + \frac{\omega^2}{v^2(\vec{x})} G(\vec{x}, \vec{x}_S; \omega) = \delta(\vec{x} - \vec{x}_S) \tag{4}$$

where $\vec{x}_S = (x_S, y_S, z_S)$ is the source position, ω is a fixed frequency. Below we describe briefly an approach which we choose to calculate the frequency domain Green's functions by the ray method.

In the tree-dimensional case, the expression for the ray-based asymptotic Green's function calculated at point R with the source in the point S is defined as [2, 18]:

$$G(R; S) = A(S, R) \exp\{i\omega\tau(S, R)\}, \tag{5}$$

where $\tau(S, R)$ is traveltime along a ray between the points S (source) and R (receiver), $A(S, R)$ is an amplitude factor provided by the ray method:

$$A(S, R) = \frac{1}{4\pi} \sqrt{\frac{v(R)}{v(S) \cdot J(S, R)}}, \tag{6}$$

$v(x)$ is a value of velocity in corresponding point of velocity model, $J(S, R)$ is geometrical spreading along a ray. The geometrical spreading is defined here by the expression

$$J = \frac{dS}{d\Omega} \tag{7}$$

where dS is the elementary oriented surface of an orthogonal ray tube section at R and $d\Omega$ is the elementary solid angle associated with the ray tube at the source. We compute finite-difference approximation of geometrical spreading factor using the theory provided in [2] (expression 3.10.33). To use this approximation of geometrical spreading we need to consider three adjacent rays with a small increment in the take-off angles as we described in the previous section. In this case, ray coverage (or ray density) within the target area should be sufficient. Amplitudes calculated along the ray tubes are interpolated on the regular grid in the same manner as the travel times. As a result, an amplitude table is obtained. Note, if ray-based travel time and amplitude tables are calculated, it is possible to calculate the Green function very quickly for any frequency because no additional raytracing is required. As an alternative to the approach outlined above, it is possible to use much more computationally expensive dynamic ray tracing [2].

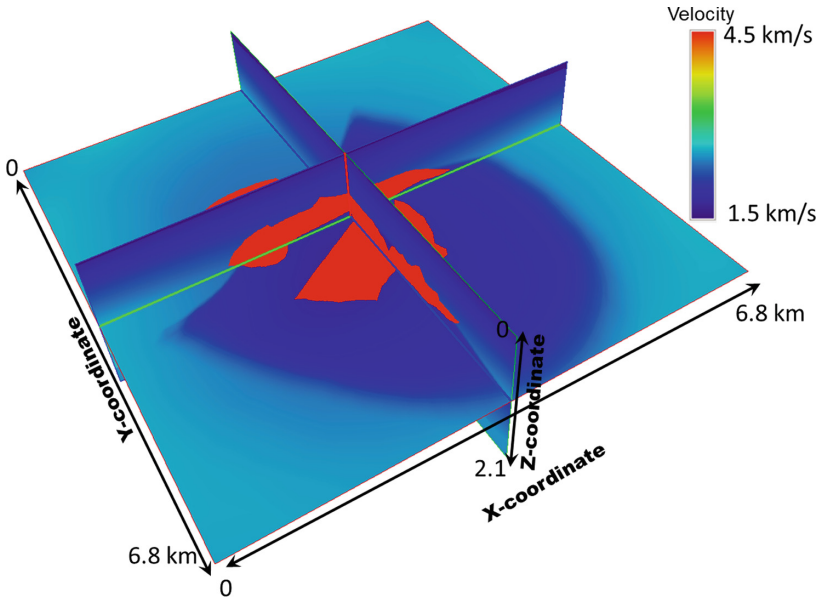

Fig. 5. Original 3D SEG Salt velocity model (scaled to the grid size 10 m). (Color figure online)

3 Numerical Examples

3.1 Travel Time Calculation in 3D SEG Salt Velocity Model

Significant problems arise when the ray method is applied in models with rapid seismic wave's velocity variations. In these cases, standard ray's behavior becomes unphysical. At sharp, non-planar boundaries the standard rays scatter and as a result "shadow" zones occur in travel times distribution. It is expected, because "by the origin" the ray method is valid if the range of velocity variations is much greater than the wavelength. In seismic

exploration applications, one of the most challenging conditions for the ray method occurs when the salt intrusions are presented in a model. Salt bodies might have a very complex shape. Seismic wave's velocity in salt is much higher than in sedimentary rocks surrounding an intrusion. Usually, it is very problematic to construct reliable rays passing through a salt body and to calculate the corresponding travel times. Below we show that "fat" rays can resolve these issues.

Figure 5 presents a well-known 3D SEG Salt velocity model [19] with a salt body of complex shape (shown in red). The model has the following parameters. Top of the model is water layer with pressure wave velocity 1500 m/s. Seismic wave velocity in salt is 4500 m/s meanwhile in surrounding area (which model sedimentary rocks) it doesn't exceed 3200 m/s. Number of grid points in each direction is $N_X = 676$, $N_Y = 676$, $N_Z = 211$ with grid steps $dx = dy = dz = 10$ m. Total spatial size of the model is $6750 \times 6750 \times 2100$ m. A point source is located in the center of the model in a point with coordinate $X_S = 3200$ m, $Y_S = 3200$ m, $Z_S = 100$ m. We want to calculate the corresponding ray based first arrival travel times in each point of the regular velocity grid (travel time table). For standard raytracing we used a code taken from well-known Madagascar freeware package. "Fat" rays are calculated using the code we developed.

Below, for "fat" ray construction we used the following parameters: "ray frequency" parameter $\upsilon = 5$ Hz, $l = 0.5$, $\theta_{max} = 0.5$, $\alpha = 1$. Number of control points was equal to 30. Figure 6a, 6b show a 3D view of 50 rays calculated for a fixed azimuth angle ($\varphi_{AZ} = 0$) and uniform dip angle increment. In Fig. 7a, 7b projections of the rays at XY plane are demonstrated (top view). One can immediately note that the standard and "fat" rays are substantially different. Behavior of "fat" rays looks much more regular. They cover much wider area of the model. Note that the rays are substantially three-dimensional. They go far beyond the plane $Y = Y_S = 3200$ m where the source is located. To calculate travel times in the whole model we must shoot the rays quite densely with small dip and azimuth angular increments. Take off angles should cover the whole intervals $\varphi_{AZ} = [0, 360°]$, $\varphi_{Dip} = [0, 360°]$. We used a bunch of 500×500 rays, i.e. the take off angles increment is 0.72°. In Fig. 8 we show travel time tables corresponding to each method. Standard rays produce "holes" in the travel time table, i.e. there are areas where the rays do not arrive at all due to complexity of the model and limitation of the ray method (at these areas travel times are zero). It is an obvious contradiction with the real physical process of wave propagation. Numerical tests proved that even the standard rays will be traced densely, this does not help to achieve adequate ray coverage everywhere. Figure 8b shows the "fat" rays travel times. "Fat" rays pass through the salt body and produce quite regularly distributed travel times. The residuals between the "fat" rays' travel times and exact first arrival travel times provided by the 3D finite difference method does not exceed 0.006 s which can be considered quite satisfactory.

If the "ray frequency" parameter increases, the "fat" rays tends to be closer to the standard rays. At a certain point (υ 30 Hz), they become indistinguishable. It is very expected behavior. Note that, for a given rays' density, "fat" ray calculation requires much more computational time than the standard ray. One of the reason is the fact that at each time step along the "fat" ray multiple accesses to the velocity model (i.e. memory access) are required to calculate the averaged velocity along the current position of the

front. The number of control points chosen for ray tracing increase the computation time almost linearly. The number of control points should be sufficient to account for the 3D velocity variation around a ray. If the number of control points is insufficient, the ray calculation can be unstable. An overabundance results in a significant increase in computational time without any visible improvement of the final result.

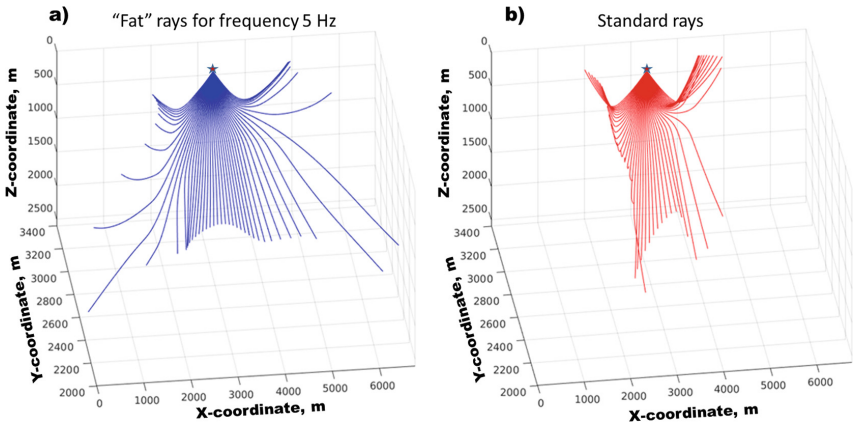

Fig. 6. 3D view of rays calculated in the original 3D SEG Salt velocity model for one source (marked as a star) and one fixed azimuth angle, $\varphi_{AZ} = 0$: a) "fat" rays calculated for the "frequency" parameter $\upsilon = 5$ Hz; b) standard rays.

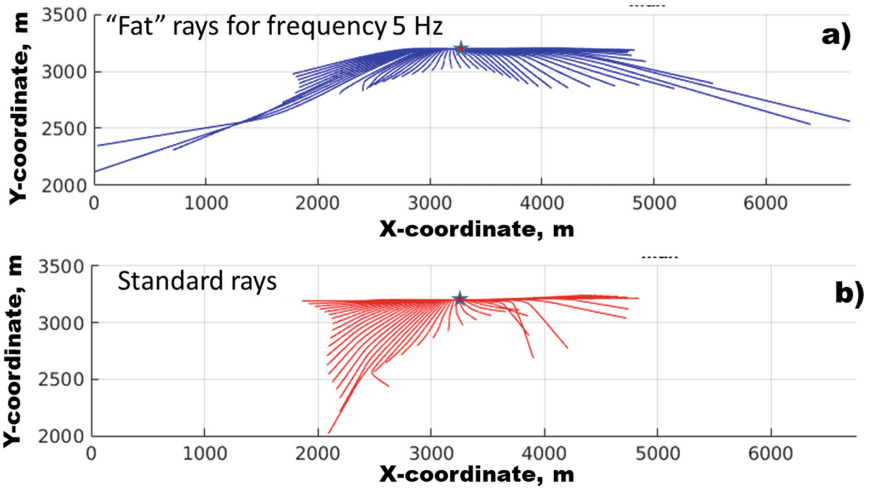

Fig. 7. Projection at XY plane of rays calculated in the original 3D SEG Salt velocity model for one fixed azimuth angle, $\varphi_{AZ} = 0$: a) "fat" rays constructed for the frequency parameter $\upsilon = 5$ Hz; b) standard rays.

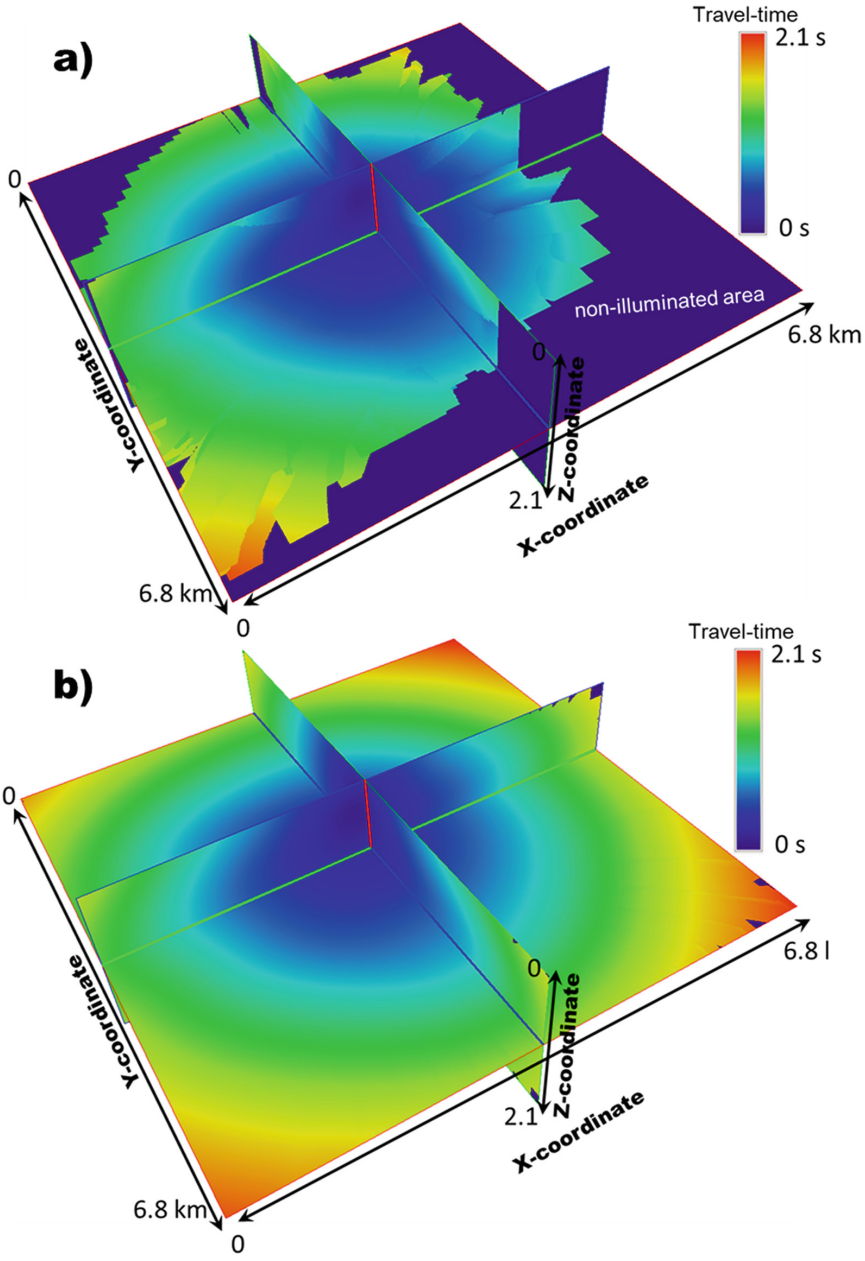

Fig. 8. Travel time table (TT) in original 3D SEG Salt velocity model: a) TT calculated using the standard rays ("shadow" zones have zero travel time); (b) TT calculated using the "fat" rays with the "frequency" parameter $\upsilon = 5$ Hz.

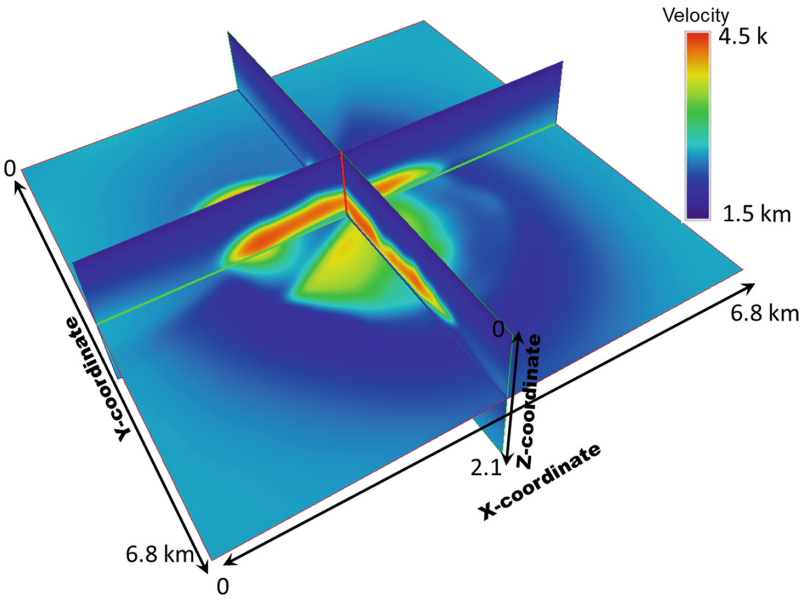

Fig. 9. Smoothed 3D SEG Salt velocity model used for acoustic wave field simulation.

3.2 Acoustic Wave Field Simulation in the Frequency Domain in Smoothed 3D SEG Salt Velocity Model

Now, we present an example of 3D acoustic wave field simulation in the frequency domain. We compare the asymptotic wave field provided by the ray method based on the "fat" rays with the "exact" wave field which is calculated by the numerical solution of Helmholtz Eq. (4). The exact wave field will contain reflected waves if the velocity model used for the simulation is non-smooth. But we apply the ray method to model first arrivals only. No reflected waves will occur in the ray-based simulation. To make the comparison of the wave fields more fair, we will use a smoothed version of the SEG Salt 3D velocity model (see Fig. 9) in order to avoid reflected waves in the "exact" wave field. The smoothed model was obtained with the spatial convolution of the original model with the 3D Gaussian function having a length of 200 m in each direction. "Exact" wave field calculation in the frequency was performed using Helmholtz iterative solver with semi-analytical preconditioner proposed in [20]. The iterative solver is applied using the same grid where the velocity model is given. The velocity model grid parameters are the same as in the previous numerical example, $N_X = 676$, $N_Y = 676$, $N_Z = 211$, $dx = dy = dz = 10$ m. Point source has coordinates $X_S = 3200$ m, $Y_S = 3200$ m, $Z_S = 100$ m. In Fig. 10a a real part of "exact" wave field at frequency 5 Hz is presented. For ray based wave field simulation we used a bunch of 500×500 rays. Even though the model is smoothed, the standard rays do not provide the required illumination for the calculation of the amplitudes. Standard rays leave holes in travel times and amplitude tables. "Fat" rays resolve the issue successfully. For "fat" ray calculation we use the same parameters as in previous example:$\upsilon = 5Hz$, $l = 0.5$, $\theta_{max} = 0.5$, $\alpha = 1$. In Fig. 10b we present "fat" rays - based wave field for frequency 5 Hz in comparison with

"exact" wave field (Fig. 10a). One can observe good fit between them. In Fig. 11, we compare the vertical and horizontal sections of the wave fields from Fig. 10 for the finite difference solution (shown in blue) and for the "fat" rays (red). The traces were taken at the plane Y = 2000 m. Quite satisfactory match is obvious. The solution error provided by "fat" rays in comparison with "exact" solution does not exceed 8% even for such a complex model as 3D SEG salt model.

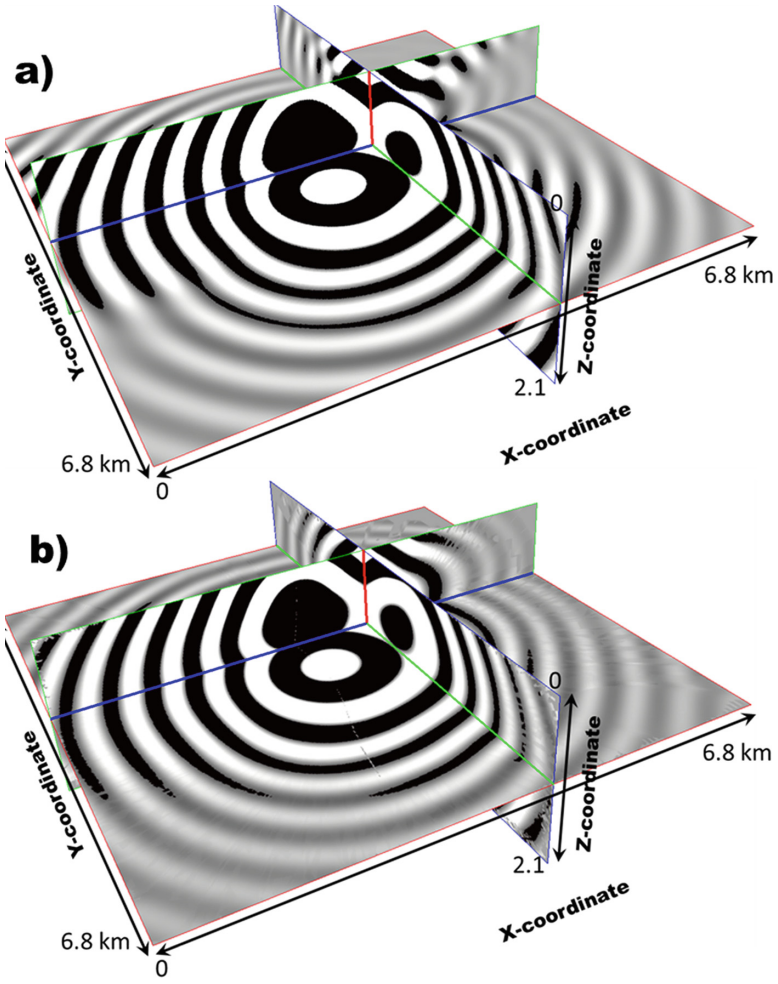

Fig. 10. Frequency domain acoustic wave fields for frequency 5 Hz (real part): a) obtained by solution of Helmholtz equation ("exact" wave field); (b) simulated using the "fat" rays. (Color figure online)

All computations presented above are performed on a personal desktop computer with Intel Core i7-3770K 3.50 GHz CPU (4 core) and 32 Gb RAM. The total cycle of "fat ray"-based Green function calculation for one source takes ~6 min of total computation

time (all 4 CPU core was used). The most time consuming part is raytracing. It takes almost 85% of total time. "Exact" wave field simulation using highly optimized iterative solver [20] requires ~7 min in the same setup (the same grid, number of CPU cores, etc.). The computation time for the "exact" solver will increase considerably with the frequency of the simulation increase. For example, for frequency of 10 Hz and 20 Hz "fat ray"-based Green function calculation for one source take ~6 min for both also, while "exact" wave field simulation using highly optimized iterative solver requires minimum 20 min for 10 Hz. We note also, if ray-based travel time and amplitude tables are ready, Green function for high frequencies can be computed very fast (seconds). There is no need to repeat ray tracing procedure.

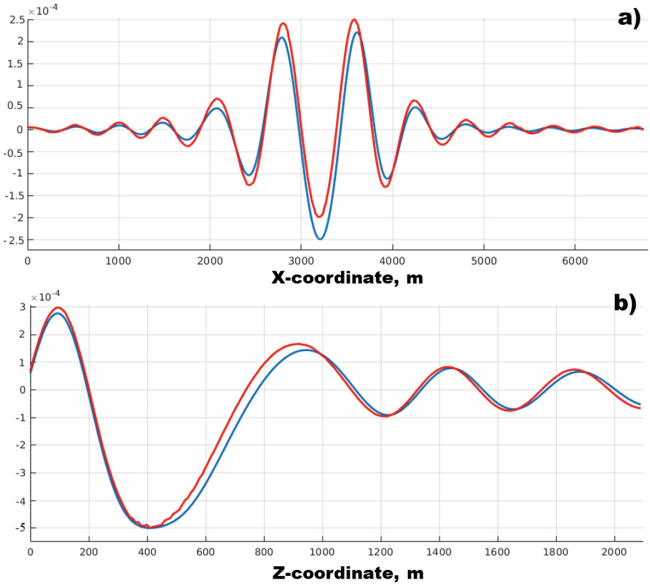

Fig. 11. 1D sections of 3D wave fields form Fig. 10.: a) horizontal (Z = 1000 m) sections; (b) vertical (X = 2000 m) sections. Exact (finite difference) wave field is shown in blue, "fat" ray based wave field is shown in red.

4 Conclusions

We consider a concept of "fat" rays for approximation frequency-dependent signal propagation in three dimensional media. "Fat" ray computation consists of two main ingredients: 1) local velocity smoothing along a 2D plane wave front; 2) control points movement to determine a wave front orientation at a next point on the ray. The procedure approximates propagation of a local plane fragment of the wave front. Ray properties depends on velocity distribution in some sub-volume around the ray and on wavelength in each point. We perform a comparative analysis of the "fat" rays versus the standard rays for calculating travel times in complex media. It shows that "fat" rays are more

stable than the standard rays and can provide reliable travel times when the standard ray method fails. Using the "fat" rays we simulate frequency domain acoustic wav field and compare it with the "exact" wave field provided by the solution of Helmholtz equation. This comparison showed a satisfactory agreement between the quality of the results. "Fat" rays wave filed in comparison with "exact" solution does not exceed 8% even for such a complex model as 3D SEG salt model. Comparison of the computational times show that "fat" rays approach needs much less (up to several orders for high frequencies) resources than Helmholtz solver. Such numerical results provide the promise of using the concept of "fat" rays in seismic exploration in a complex three-dimensional environment.

Acknowledgments. The reported study was funded by RFBR and GACR, project number 20-55-26003.

References

1. Babich, V.M., Buldyrev, V.S.: Asymptotic Methods in Short-Wavelength Diffraction Theory. Alpha Science (2009)
2. Cerveny, V.: Seismic Ray Theory. Cambridge University Press, Cambridge (2001)
3. Kravtsov, Y.A., Orlov, Y.I.: Geometrical Optics of Inhomogeneous Media. Springer, Heidelberg (1990)
4. Ben-Menahem, A., Beydoun, W.B.: Range of validity of seismic ray and beam methods in general inhomogeneous media –I. General theory. Geophys. J. Int. **82**, 207–234 (1985)
5. Marquering, H., Dahlen, F.A., Nolet, G.: Three-dimensional sensitivity kernels for finite-frequency traveltimes: the banana-doughnut paradox. Geophys. J. Int. **137**, 805–815 (1999)
6. Dahlen, F.A., Hung, S.-H., Nolet, G.: Fréchet kernels for finite-frequency traveltimes—I. Theory. Geophys. J. Int. **141**, 157–174 (2000)
7. Cerveny, V., Soares, J.E.P.: Fresnel volume ray tracing. Geophysics **57**, 902–915 (1992)
8. Lomax, A.: The wavelength-smoothing method for approximating broad-band wave propagation through complicated velocity structures. Geophys. J. Int. **117**, 313–334 (1994)
9. Vasco, D.W., Peterson, J.E., Majer, E.L.: Beyond ray tomography: wavepaths and Fresnel volumes. Geophysics **60**, 1790–1804 (1995)
10. Bube, K.P., Washbourne, J.K.: Wave tracing: ray tracing for the propagation of band-limited signals: part 1 – theory. Geophysics **73**, VE377–VE384 (2008)
11. Yarman, C.E., Cheng, X., Osypov, K., Nichols, D., Protasov, M.: Band-limited ray tracing. Geophys. Prospect. **61**, 1194–1205 (2013)
12. Vasco, D.W., Nihei, K.: Broad-band trajectory mechanics. Geophys. J. Int. **216**, 745–759 (2019)
13. Foreman, T.L.: An exact ray theoretical formulation of the Helmholtz equation. J. Acoust. Soc. Am. **86**, 234–246 (1989)
14. Protasov, M., Gadylshin, K.: Computational method for exact frequency-dependent rays on the basis of the solution of the Helmholtz equation. Geophys. J. Int. **210**, 525–533 (2017)
15. Neklyudov, D., Protasov, M.: Acoustic wavefields simulation by the ray method with approximation of a broadband signal propagation. In: Gervasi, O., Murgante, B., Hendrix, E.M.T., Taniar, D., Apduhan, B.O. (eds.) ICCSA 2022. LNCS, vol. 13376, pp. 84–96. Springer, Cham (2022). https://doi.org/10.1007/978-3-031-10450-3_7

16. Jordi, C., Schmelzbach, C., Greenhalgh, S.: Frequency-dependent traveltime tomography using fat rays: application to near-surface seismic imaging. J. Appl. Geophys. **131**, 202–213 (2016)
17. Bulant, P., Klimeš, L.: Interpolation of ray theory traveltimes within ray cells. Geophys. J. Int. **139**(2), 273–282 (1999)
18. Lucio, P.S., Lambaré, G., Hanyga, A.: 3D multivalued travel time and amplitude maps. PAGEOPH **148**, 449–479 (1996)
19. Aminzadeh, F., Burkhard, N., Long, J., Kunz, T., Duclos, P.: Three dimensional SEG/EAGE models - an update. Lead. Edge **15**(2), 131–134 (1996)
20. Belonosov, M., Dmitriev, M., Kostin, V., Neklyudov, D., Tcheverda, V.: An iterative solver for the 3D Helmholtz equation. J. Comput. Phys. **345**, 330–344 (2017)